Fatigue Damage of Designed T-type Specimen under Different Proportion Repeating Two-Step Variable Amplitude Loads

Jin Gan[a,c*], Kai Zhao[b], Zhou Wang[d], Xiaoli Wang[d], Weiguo Wu[a]

[a] Department of Naval Architecture, Ocean and Structural Engineering, School of Transportation, Wuhan University of Technology, Wuhan 430063, P. R. China;

[b]Wuhan Institute of Marine Electric Propulsion, Wuhan 430064, P. R. China;

[c] Department of Mechanical Engineering, University of Bristol, Bristol BS8 1TR, UK

[d] Department of Automotive Engineering, School of Automotive Engineering, Wuhan University of Technology, Wuhan 430070, P. R. China

Abstract: In order to investigate the fatigue damage evolution of typical joints of River-Sea-Going Ship (RSGS) under a repeating two-step variable amplitude (VA) loading condition, and to estimate the influence of the damage of low amplitude load below the fatigue limit and the interaction effect between the high and low amplitude loads on the fatigue life of the structure, a series of fatigue experiments of designed T-type specimen (DTS) under different repeating two-step VA loading conditions were carried out in this work, which are designed according to hull structure characteristics and actual service conditions of RSGS. The experimental results show that the interaction damage value (D_{nl}) firstly increases and then decreases with increasing the cycle ratio of low to high amplitude load from 1 to 5. The value of D_{nl} is negative when the cycle ratio is relatively large, not less than 4.5 in the current study, which indicates that the effect of loading interaction not only doesn't cause damage but has a beneficial effect on the fatigue life of the DTS. The X-ray Diffraction (XRD) analysis was carried out subsequently at the fatigue crack initiation region with the aim of confirming the material characteristic at the microcrack tip changing from work-hardening state to work-softening state with the cycle ratio increasing.

Key words: River-Sea-Going Ship; fatigue damage; repeating two-step VA loading; interaction damage value; X-ray Diffraction analysis.

[*]**Corresponding author:** Jin Gan **Tel:** +86 150-7236-6677

E-mail address: ganjinwut@163.com (Jin Gan)

Nomenclature	
σ_i	Stress at load step i
σ	Stress
n_i	Number of cycles accumulated at load step i
$N_i,\ N_L,\ N_H$	Number of cycles to failure with constant amplitude stress $\sigma_i,\ \sigma_L,\ \sigma_H$
D	Cumulative fatigue damage
E	Young's modulus
σ_Y	Yield stress
σ_{UTS}	Ultimate tensile stress
σ_f	Fatigue limit
ρ	Density of material
γ	Poisson's ratio
$n_L,\ n_H$	Number of cycles with stress $\sigma_L,\ \sigma_H$ in each block
$\sigma_L,\ \sigma_H$	Maximum amplitude of the stress below and above fatigue limit in the block
F	Input load of the MTS
$\Sigma n_L,\ \Sigma n_H$	The total number of cycles to failure with stress $\sigma_L,\ \sigma_H$
D_{nl}	Loading interaction damage value
σ_0	Yield stress of the annealed metal
μ	Shear modulus
b	Burgers vector of dislocations
ρ_D	Dislocation density
β, A	Constant of material
m	Negative slope of S-N curve

1. Introduction

The steel components in ship and offshore structures are often subjected to cyclic load during their service life, so the assessment of the fatigue life and fatigue property of these components is crucial to the safety of ship and offshore structures [1]. There are numerous research works [2-5] focusing on the experimental and theoretical investigation of fatigue life and fatigue properties. Most of studies [6-8] are related to constant amplitude (CA) loading conditions due to the limitations in experimental techniques and theoretical principles, even though the cyclic load is not constant but variable in most cases of ship and offshore structures. River-Sea-Going Ship (RSGS) is one kind of advanced ship navigating between the Yangtze river and coastal waters in China without changing any equipment and transit link [9-11]. The variable amplitude (VA) cyclic load due to the different wave loads of the inland river and the sea is the most common service condition of RSGS steel components [12, 13].

The Palmgren–Miner linear damage rule is a common method to estimate fatigue damage of steel components [14, 15]. The fatigue damage D is calculated by the following relationship

$$D = \sum \frac{n_i}{N_i} \tag{1}$$

where n_i is the number of cycles accumulated at load step i, N_i is the number of cycles to failure with constant amplitude stress σ_i, and D is the total cumulative damage value at different stress

levels. Usually, when this value reaches 1, failure occurs [16]. There is no consideration for the fatigue damage of low amplitude load below the fatigue limit and the influence of load interaction under VA loads.

However, some research works [17-19] have reported that the low amplitude load below the fatigue limit leads to fatigue damage. Mayer [17] reported that the low amplitude load had a negative effect on fatigue strength if the high stress amplitude was higher than 13% above the fatigue limit and the cumulative damage was less than 1 with a low carbon steel C15E. Mayer et al. [18] also found that the low amplitude load below the fatigue limit would accelerate crack growth of cast aluminium alloy 319-T7 when the high stress value was higher than 40% of the fatigue limit. Jono et al. [19] conducted a series of experiments on smooth specimens of 0.38% carbon steel and claimed that the number of low amplitude stress loads below the fatigue limit in the VA loading block had a negative effect on its fatigue properties. In addition, some other researches also showed the fatigue strength and fatigue life could be increased by introducing a low amplitude load [20-22]. Xi et al. [20] investigated the strengthening effects of low amplitude load below the fatigue limit on the fatigue strength of transmission gears via surface heat treatment. The results showed that the low amplitude load, which was from 75% to 95% of fatigue limit, had a remarkable strengthening effect. They also found the fatigue strength of vehicle components improved significantly by applying different cycles of low amplitude loads in their following work [21] and there was an optimum strengthening cycle of low amplitude load.

Previous studies have shown that the low amplitude load below the fatigue limit has different strengthening or damage effects in different loading conditions. In fatigue analysis, not only the cumulative damage due to a small amplitude load below the fatigue limit should be considered to assess the fatigue life of steel structures, but also the interaction effect between the high and low amplitude loads on the fatigue life of steel structures. To overcome the issues of Miner's rule, some nonlinear cumulative damage models were proposed to analyze the fatigue properties of structures under VA loads. Pereira et al. [23] assessed the relationship between cyclic elastoplastic behaviors and damage accumulation of the P355NL1 steel based on VA fatigue tests, and illustrated the nonlinearity of damage. Rege and Pavlou [24] developed a new nonlinear fatigue model according to the S-N curves, while the fatigue life below inflection point is treated as infinite. M. Ciavarella et al. [25] obtained the Gassner curves under random VA loads based on the CA S-N curve and the Critical Distance Method, but the load interaction between large loads above the fatigue limit and small loads below the fatigue limit wasn't considered. By introducing load interaction factor, Lv et al. [26] proposed a modified nonlinear model based on Ye and Wang's original model [27] to analyze fatigue damage of smooth and notched specimens under two-stage loading. Correia et al. [28] applied the probabilistic method to the double linear damage rule considering the sequential effect of load. The proposed method could explain the fatigue test results of P355NL1 under load block effectively. Recently, Zhu et al. [29] compared five different nonlinear damage models and proposed a new non-linear fatigue damage model considering the effect of load sequence and interaction, which was more accurate than other models in predicting fatigue life. Although the aforementioned nonlinear fatigue cumulative damage models give reasonable predictions for specific load blocks or spectra, few of them have considered the effects of small loads below the fatigue limit and the interaction of repeating two-step load. Besides, the fatigue performance under two- step VA load is not clearly explained from the view of material science.

As nearly 80% of the routes of RSGS are on the river, the most cyclic loads of the steel structure

are below the fatigue limit. The correct assessment of the effect of low amplitude load and the interaction effect between the high and low amplitude loads on the fatigue property of steel component is very critical for calculating the fatigue life of RSGS structure. Therefore, an investigation of the fatigue damage evolution of designed T-type specimen (DTS) based on the characteristics of RSGS structural components was carried out in this work. The load spectrum was repeating two-step VA load, which was according to the actual loading condition of RSGS. Firstly, different CA loading fatigue tests were carried out on the DTS. Then, the fatigue tests under repeating two-step variable VA load were carried out. According to the fatigue test results, a modified Palmgren–Miner rule was proposed by considering the effect of the damage of low amplitude load below the fatigue limit and the interaction effect between the high and low amplitude stress loads on the fatigue life of the structure. Finally, the X-ray Diffraction (XRD) analysis was carried out with the aim of analyzing the material characteristic variation at the microcrack tip with the load cycle ratio increasing.

2. Experimental setup

2.1. Material

Q345B steel, which is one of the most common structural materials used in RSGS, was chosen as a research object in this work. Q345B steel is a low carbon steel with good corrosion resistance and relative high strength. The chemical composition of Q345B steel is shown in Table 1**.** The Q345B steel specimen was quenched, first tempered at 930℃ for 2 hours, and second tempered at 400℃ for 50 minutes followed by cooling in the air. The mechanical properties of Q345B steel are shown in Table 2**.**

Table 1. The chemical composition of Q345B steel

Element	C	Mn	Si	S	P	Ni	Cr	Mo	V	Cu	Fe
Composition (wt%)	0.17	0.82	0.23	0.014	0.021	0.011	0.014	0.007	0.004	0.039	Balance

Table 2. The mechanical properties of Q345B steel

Material	E(GPa)	σ_Y(MPa)	σ_{UTS}(MPa)	ρ (g/cm^3)	ν
Q345B	206	320.43	480.58	7.85	0.26

2.2. Specimen

The fatigue failure of ship structure mainly occurs in typical joints, such as bending angle structure, the end structure and free edge of structure. By analyzing, we find that the joint forms all have similar vertical stepped structure type. Fatigue crack initiation is induced by the local stress concentration caused by the sudden change of geometric form. Therefore, the ideal T-type specimen is designed. Fig. 1 shows the geometric dimension of the DTS. The specimen consists of two cross sections with thicknesses of 8 mm and 22 mm, respectively. The combination of wire cut electrical discharge machining (WEDM) and laser cutting was used to ensure the specimens' dimensional accuracy. Stress concentration is easy to occur where the cross section changes. Therefore, fatigue failure always appears in this changing area.

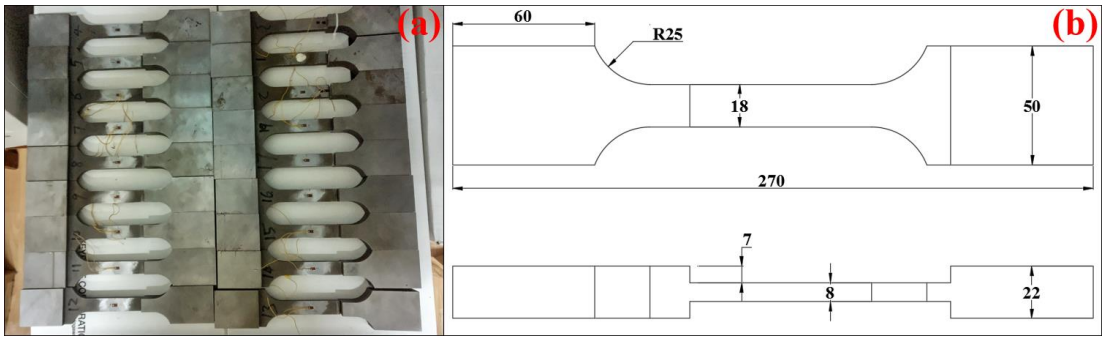

Fig. 1. The DTS for fatigue test **(a)** and geometric dimension of the DTS **(b)**

2.3. Fatigue tests experimental setup

All the loading-controlled fatigue tests were carried out at room temperature with MTS322 250 kN Dynamic Fatigue Testing System at the Ship Structure Laboratory of Wuhan University of Technology (Wuhan, China). Fig. 2 shows the overall layout of MTS322 facility setup (a) and the clamping state of the specimen in fatigue test (b). The fatigue test device consists of a loading frame (1) and a hydraulic clamping system (2), which are used to provide vertical cyclic loads in the fatigue test. The hydraulic clamping system includes a symmetrically arranged wedge-shaped clamps (3), a cross sectional stress data transmission wire (4). The notch fatigue specimen (5) is fixed by the clamps during the fatigue test. According to the condition of test equipment and research purpose, the stress ratio is 0.1 and the loading frequency is 30 Hz in all CA and VA fatigue tests.

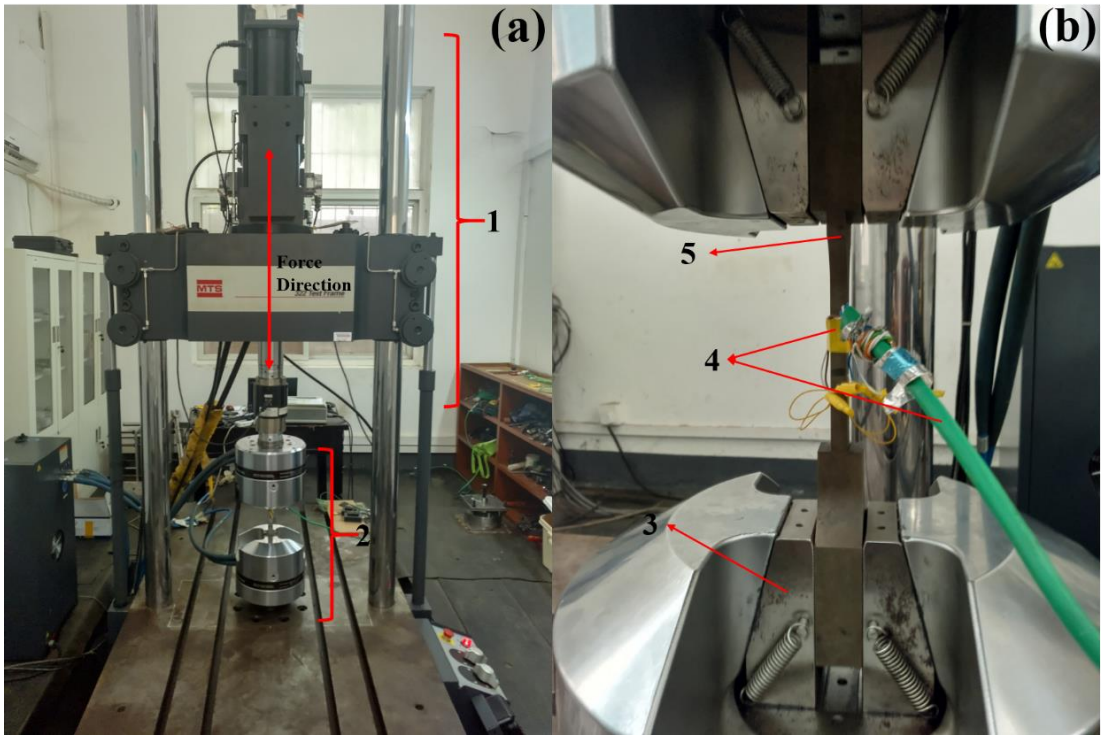

Fig. 2. MTS 322 facility setup **(a)** and the clamping state of the DTS **(b)**

Static loading tests were carried out before fatigue tests. Fig. 3 shows the arrangement of strain gauge on both sides of the fatigue specimen in static loading tests. The different setting loading values in fatigue tests were obtained according to the measured stresses in different static loading tests, which were used to ensure that the actual stresses in fatigue tests are the same as setting stresses.

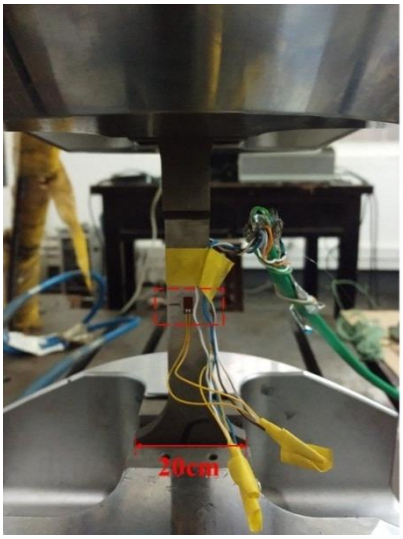

Fig. 3. Arrangement of strain gauge in static loading tests

Based on a large number of fatigue tests' results in previous work of our group, the crack propagates rapidly after the macroscopic crack is observed. The number of cycles of the macrocrack propagation is only about 10^2~10^3. Therefore, the fatigue crack initiation life can be regarded as the whole fatigue life of the specimen. Keyence VHX-5000 digital microscope, which is capable of 50–450x optical zoom levels, was used to observe the fatigue fracture of the DTS. Fig. 4a shows the arrangement of fracture analysis for the DTS after fatigue failure. Fig. 4b shows the fracture morphology of the notched fatigue specimen with 235 MPa CA loading. In Fig. 4b, it is very clear to distinguish the crack initiation area, the crack propagation area and the final rupture area in fatigue fracture of the DTS. The color in Fig. 4b represents the distance from the lowest point in the Z direction. The red line represents the crack propagation direction during the fatigue test.

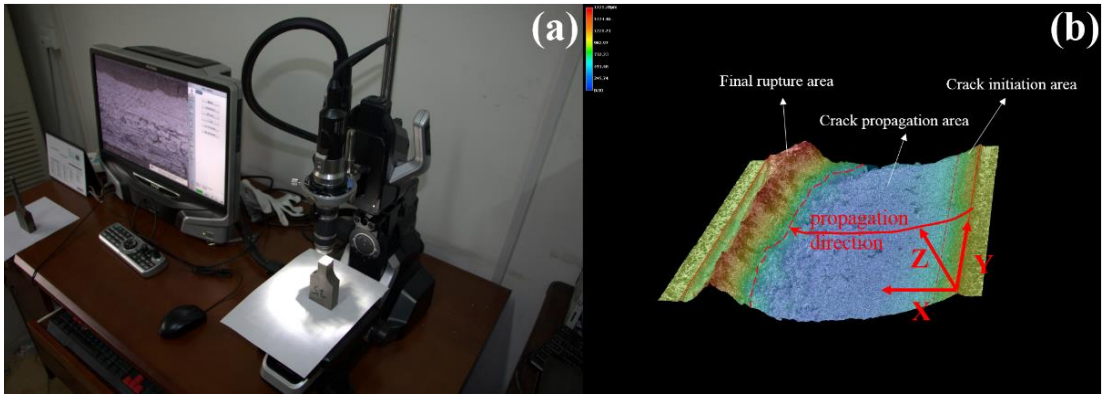

Fig. 4. The arrangement of fracture analysis for the DTS **(a)** and the fracture morphology of the DTS with 235 MPa CA loading **(b)**

2.4. CA loading fatigue test procedure

As the service environment of RSGS is a combination of river wave load and sea wave load, the fatigue tests with CA load above and below the fatigue limit were carried out on the DTS, respectively. According to the actual stress magnitude of the RSGS structure sailing along the coastal route and the Yangtze River of China, the cyclic load above the fatigue limit is set to 235 MPa, and the cyclic load below the fatigue limit is set to 100 MPa, respectively. In order to obtain

the CA fatigue life by the S-N curve (Wholer curve) of the DTS, multiple groups of CA load fatigue tests were carried out firstly. Each group of tests contains at least three or more valid data. As 10^7 is always chosen as the number of cycles to represent the fatigue limit of materials in engineering, the fatigue test is stopped when the number of cycles is 10^7 even if the fatigue failure doesn't occur in our fatigue test. Based on the fitted Wholer curve, the fatigue life under different constant amplitude stresses can be obtained by an interpolation method.

2.5. VA loading fatigue test procedure

In order to analyze influence of the damage of low amplitude load below fatigue limit and the interaction effect between the high and low amplitude loads on the fatigue life of the structure, repeating two-step VA loading fatigue tests were carried out after CA loading fatigue tests. The high amplitude load σ_H was 235 MPa and the low amplitude load σ_L was 100 MPa. Fig. 5 shows the load spectrum of the repeating two-step VA loading fatigue test. The number of cycles in one block was 40000 in all VA loading fatigue tests. Five groups of VA loading fatigue tests with different cycle ratios (n_L/n_H) in one block were carried out. Table 3 shows the serial number of fatigue specimens in different repeating two-step VA load conditions.

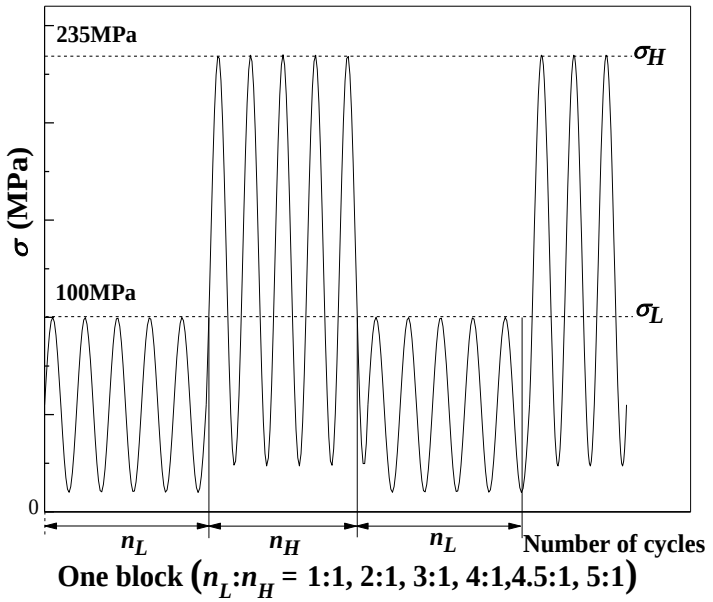

Fig. 5. Load spectrum of the repeating two-step VA loading fatigue test

Table 3. Two-step VA fatigue tests under different cycle ratio which were 1:1, 2:1, 3:1, 4:1, 4.5:1 and 5:1

Specimen No.	n_L/n_H	First step		Second step	
		σ_L (MPa)	n_L	σ_H (MPa)	n_H
12,13,14,15	1:1	100	20000	235	20000
16,17,18,19,20	2:1	100	26667	235	13333
21,22,23,24	3:1	100	30000	235	10000
25,26,27	4:1	100	32000	235	8000
28,29,30	4.5:1	100	32727	235	7273
31,32,33,34	5:1	100	33333	235	6667

2.6. The X-ray Diffraction (XRD) analysis

In order to investigate the micro mechanical property of crack initiation area and analyze the reason for the effect of loading interaction on fatigue damage variation with cycle ratio increasing, the X-ray Diffraction (XRD) analysis of crack initiation area was carried out via D8 Advance diffractometer（Wuhan University of Technology, Material Research and Testing Center）with CuK radiation, voltage 40 kV and current 40 mA. The scanning mode of XRD analysis was continuous scanning mode. The scanning step is 0.01° and the scanning speed is 10°/min. The work-hardening state and work-softening state of fatigue crack initiation area were characterized by XRD analysis with the aim of explaining the interaction effect between the high and low amplitude loadings on the fatigue life of the DTS.

3. Test results

3.1. Static loading test result

Before the fatigue test, static loading test was carried out for each specimen in order to obtain accurate load input values. Fig. 6 shows the Load-Stress curves of static loading test for all 34 fatigue test specimens. The X-axis represents the input load of MTS and the Y-axis represents the real load stress. Each Load-Stress curve was obtained by linear fitting of eight data points. According to the static loading test result, it can be seen that the difference of stress value in different fatigue test specimen does not exceed 10 MPa under the same load. All the Load-Stress curves are linear and similar to each other, which indicates the geometric dimension and the machining quality of all DTS are good. According to the Load-Stress curve obtained by the static load test, the loading force input into the MTS of each fatigue test is obtained by interpolation method.

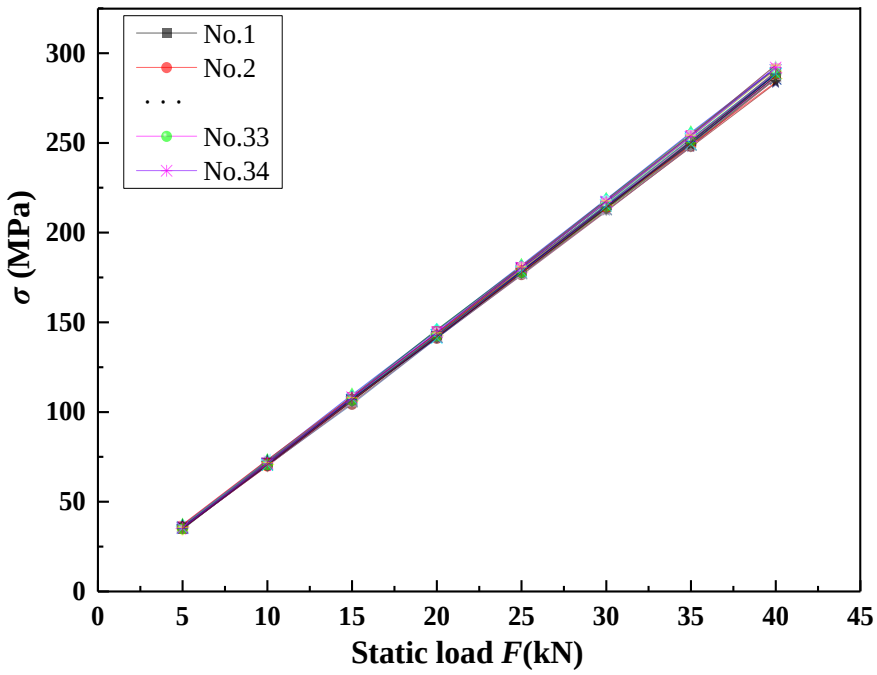

Fig. 6. The Load-Stress curves of static loading test for all 34 fatigue test specimens

3.2. CA loading fatigue test result

In fatigue test, more than one abnormal data always appears because of many influence factors such as material microstructure, material flaws, the material processing technology and so on. Therefore, some method should be carried out to delete the abnormal data with the aim of making the experimental data more reliable. Compared with other methods of eliminating the abnormal test data, the method of Chauvenet criterion is more suitable for limited quantity of data [30]. According to the Chauvenet criterion, some invalid data of fatigue tests under the same stress was excluded. The fitted double logarithmic S-N curve (Wholer curve) is shown in Fig. 7 and the fitted equation of this S-N curve can be expressed as follows

$$\lg N = 21.028 - m\lg\sigma_{max} \tag{2}$$

where *m* is the negative slope of the Wohler curve. There are different analytical methods for fatigue life of small load below the fatigue limit, as shown in the Fig. 7. The classical Miner's rule does not take into account the damage effect of small loads below the fatigue limit. As mentioned in the reference [25], the "Palmgren-Miner-Elementary method" states that the slope below the knee point is consistent with the slope above the fatigue limit, and the Haibach method recommends a negative slope of *2m-1*. Compared with other methods, the Haibach method does not analyze the results overly conservatively, and meanwhile considers the damage effect of small loads below the fatigue limit. So the Haibach method is adopted to consider the damage caused by low amplitude stress below the fatigue limit.

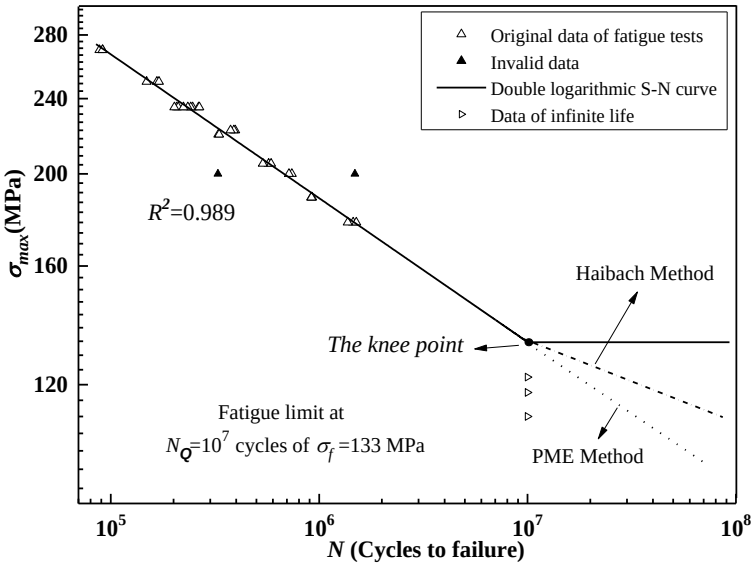

Fig. 7 The double logarithmic S-N curve under CA loads of DTS

3.3. Two-step repeating VA loading fatigue test result

Table 4 shows the fatigue test results of six VA loading groups with different cycle ratios (n_L/n_H). The cycle ratios in one block are 1:1, 2:1, 3:1, 4:1, 4.5:1 and 5:1 respectively. The value of $\sum n_L$ is the total cyclic number of low amplitude stress σ_L. The value of $\sum n_H$ is the total cyclic number of high amplitude stress σ_H. Therefore, the value of $\sum(n_H+n_L)$ stands for the total cyclic number of the DTS during repeating two-step VA loading fatigue test. Similar to the above mentioned CA load fatigue test, the VA fatigue test data is also dispersive. In order to avoid accidental error, the fatigue tests of each group were conducted more than three times to ensure the accuracy of the data. Fig. 8

shows the scatter data of repeating two-step VA loading fatigue test. According to the method of Chauvenet criterion, some tests data (No.12, No.20, No.23 and No.31) are excluded as invalid data. When the confidence level is 97.56%, all the VA fatigue test data after eliminating the abnormal data are in the range of confidence limits. The fatigue lives of specimens No.12 and No.20 are larger than other specimens under the same loading condition, which is probably due to the introduction of compressive residual stress near the notch in actual manufacturing practice. In terms of No.31, the slightly asymmetric notch was found and the asymmetric structure may lead to more obvious stress concentration on one side of DTS.

Table 4. VA loading test results of the DTS

Specimen No.	n_L/n_H	First step		Second step		$\sum(n_H+n_L)$
		σ_L (MPa)	$\sum n_L$	σ_H (MPa)	$\sum n_H$	
12	1:1	100	400000	235	396342	796342
13	1:1	100	220000	235	204549	424549
14	1:1	100	260000	235	257533	517533
15	1:1	100	200000	235	196964	396964
16	2:1	100	373324	235	180509	553833
17	2:1	100	399990	235	187099	587089
18	2:1	100	533320	235	258642	791962
19	2:1	100	533320	235	261009	794329
20	2:1	100	799980	235	389758	1189732
21	3:1	100	540000	235	172153	712153
22	3:1	100	540000	235	173870	713870
23	3:1	100	480000	235	156113	636113
24	3:1	100	570000	235	183434	753434
25	4:1	100	640000	235	159360	799360
26	4:1	100	576000	235	143723	719723
27	4:1	100	736000	235	182522	918522
28	4.5:1	100	1047296	235	226833	1274129
29	4.5:1	100	1047296	235	225992	1273288
30	4.5:1	100	1145480	235	250784	1396264
31	5:1	100	966657	235	191637	1158294
32	5:1	100	1199988	235	236540	1436528
33	5:1	100	1366653	235	271102	1637755
34	5:1	100	1366653	235	272259	1638912

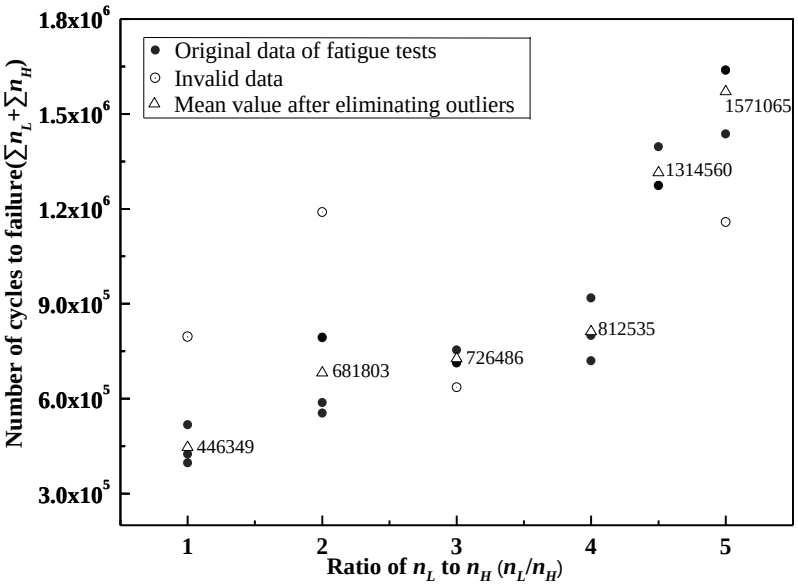

Fig. 8. Two-step VA loading fatigue tests scatter data under different cycle ratio

It is not reasonable to directly compare the total number of cycles to failure in two-step VA loading fatigue tests with CA loading fatigues, since the low amplitude load is so small in two-step VA loading fatigue tests and the corresponding number of cycles ($\sum n_L$) cannot be counted. Therefore, more details are discussed in Section 4 to evaluate the benefit effect of the amplitude load below the fatigue.

3.4. Fracture morphology

Fig. 9 shows the macroscopic fracture surface topography **(a)** and the microscopic topography of fatigue crack initiation area **(b)** in the CA loading fatigue test with the load of 235 MPa. In Fig. 9a, the upper part of the fracture is the fatigue crack initiation area, the middle part is the crack propagation area and the lower part is the transient breaking area. Fig. 9b shows the microstructure of the fatigue crack initiation area, it can be seen that there is more than one crack initiation site in the fatigue crack initiation area. According to the fatigue test results in our work, not all fatigue crack initiation leads to crack propagation during the cyclic loading process. Fig. 10 shows the macroscopic fracture surface topography **(a)** and the microscopic topography of fatigue crack initiation area **(b)** in the VA loading fatigue test with the load cycle ratio (n_L/n_H) of 1:1 and the value of 100 MPa/235 MPa. By comparing Fig. 9a with Fig. 10a, it can be seen that the macroscopic fracture surface topography are similar in the CA and VA loading conditions. Because of the stress concentration at the cross section variation area, the crack initiation areas of these two conditions are both at the edge of this area. By comparing Fig. 9b with Fig. 10b, it can be seen that the number of crack initiation sites under the VA load is obviously more than that under the CA load. This phenomenon indicates the low amplitude load below the fatigue limit has a promoting effect on the micro crack nucleation.

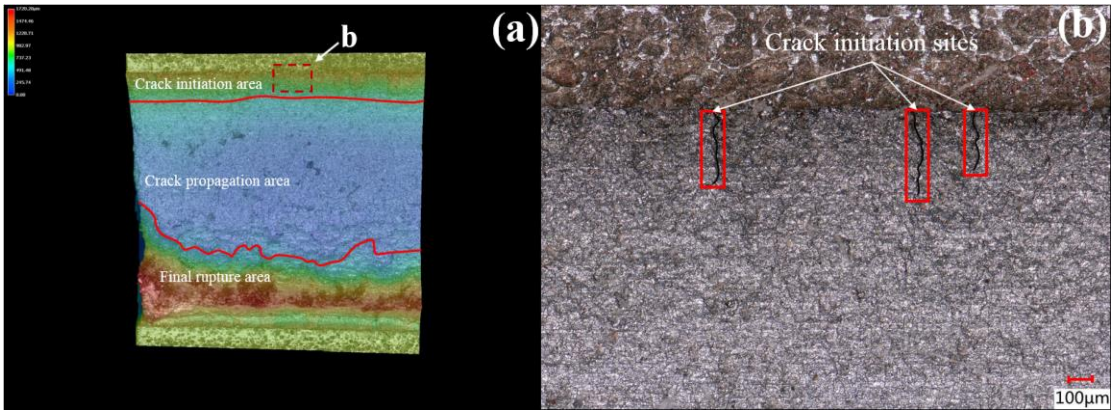

Fig. 9. The macroscopic fracture surface topography **(a)** and the microscopic topography of fatigue crack initiation area **(b)** in the CA load fatigue test with the load of 235 MPa

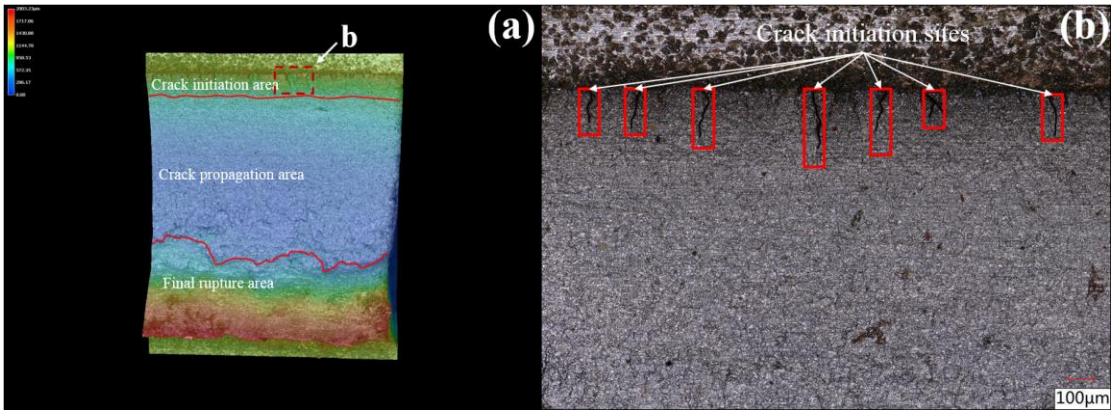

Fig. 10. The macroscopic fracture surface topography **(a)** and the microscopic topography of fatigue crack initiation area **(b)** in the VA load fatigue test with the load cycle ratio of 1:1 and the value of 100 MPa/235 MPa

4. Modified Miner rule considering loading interaction effect

According to the Palmgren-Miner linear damage rule, the fatigue cumulative damage fraction is 1 when the fatigue failure occurs. Furthermore, the fatigue damage of the low amplitude load below the fatigue limit is not considered because the CA fatigue life below the fatigue limit is infinity. However, as we mentioned previously, some studies [31] have shown that fatigue damage of low amplitude loading can't be ignored. Table 5 shows the values of fatigue cumulative damage fraction considering the damage of low amplitude load below the fatigue limit and the interaction damage due to the interaction effect between the high and the low amplitude loads for different cycle ratios in VA loading conditions.

From Table 5, it can be seen that the value of fatigue cumulative damage (D) is less than 1 when n_{L}/n_H is not greater than 4, meanwhile the value of D is larger than 1 when n_{L}/n_H is more than or equal to 4.5. Even if considering the damage caused by the low amplitude load below the fatigue limit, the similar rule still exists but the values of D in different cycle ratio conditions are larger. Fig. 11 shows the variation of cycle numbers of low amplitude load and high amplitude load with the cycle ratio increasing.

Table 5. Cumulative fatigue damage under different cycle ratios two-step VA loads

Cycle ratio	Low-amplitude		High-amplitude		Value of cumulative fatigue damage (D)		D_{nl}
	σ_L (MPa)	$\sum n_L$	σ_H (MPa)	$\sum n_H$	according to Miner rule	considering low-amplitude stress (Haibach method)	
1:1	100	226667	235	219682	0.943	0.943	0.057
2:1	100	459988	235	221815	0.952	0.953	0.047
3:1	100	550000	235	176486	0.757	0.759	0.241
4:1	100	650667	235	161868	0.695	0.697	0.303
4.5:1	100	1080024	235	234536	1.006	1.010	-0.011
5:1	100	1311098	235	259967	1.115	1.120	-0.120

From Fig. 11, it can be seen that the cycle number of low amplitude load increases with the cycle ratio increasing. However, the cycle number of high amplitude loads decreases firstly and then increases with the cycle ratio increasing. When the cycle ratio is 5, both the cycle numbers of low amplitude load and high amplitude load reach their maximum values in all different cycle ratio conditions in fatigue tests. From Table 5, it can also be seen that the cumulative damage value caused by the low amplitude load and the high amplitude load decreases firstly and then increases with the cycle ratio increasing. This interesting phenomenon indicates that the fatigue life of the DTS in repeating two-step VA loading condition can't be predicted accurately by Palmgren-Miner linear damage rule, even if the damage caused by the low amplitude load is considered.

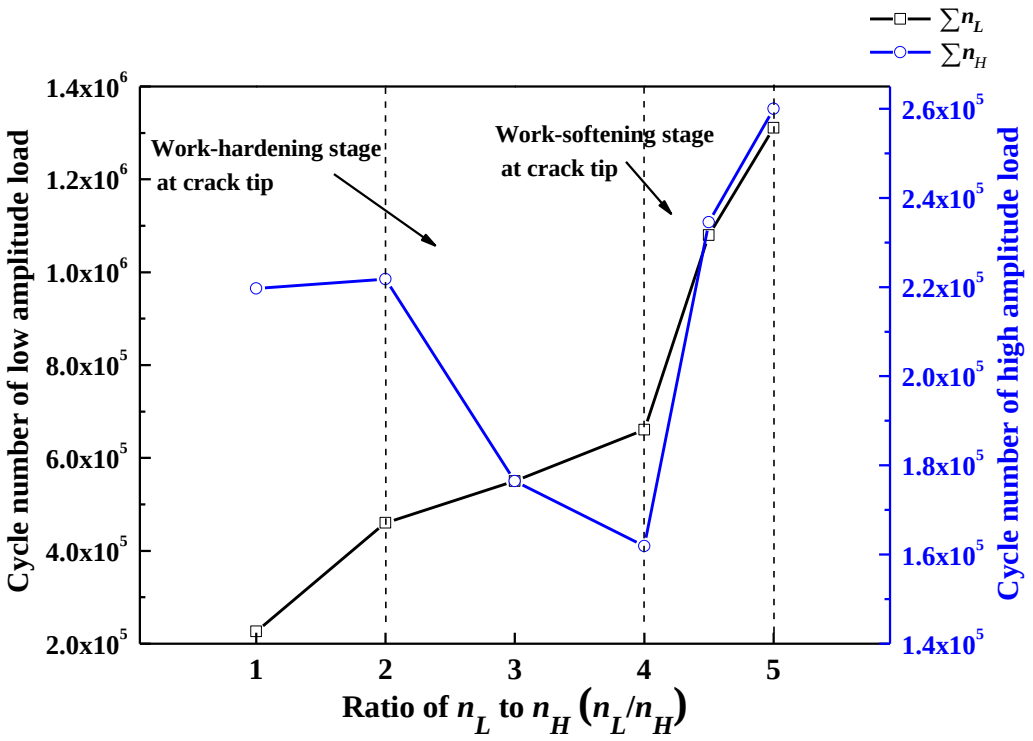

Fig. 11. The variation of cycle numbers of low amplitude load and high amplitude load with cycle ratio increasing

Some previous research results [32, 33] have already shown that the influence of the interaction effect between the high and low amplitude loads on the fatigue life cannot be ignored in the VA loading fatigue tests. In our work, the interaction damage value (D_{nl}), which reflects the interaction

effect between the high and low amplitude loads on fatigue damage, was proposed firstly to modify the Palmgren-Miner linear damage rule. Furthermore, the damage value due to the low amplitude load below the fatigue limit was introduced into the Palmgren-Miner linear damage rule as well. According to the Palmgren-Miner linear damage rule, fatigue failure occurs when the cumulative damage value D reaches 1. Therefore, the value of D_{nl} can be calculated as following:

$$D_{nl} = 1 - D = 1 - \left(\frac{\sum n_L}{N_L} + \frac{\sum n_H}{N_H}\right) \tag{3}$$

where $\sum n_L$ is the total cycle number of the low amplitude load σ_L, $\sum n_H$ is the total cycle number of the high amplitude load σ_H. N_L and N_H are the number of cycles to failure at the low and high CA load. For the ideal case of VA load condition, the small load cycle is infinitely close to zero, and almost all of the load cycle is large load, which is equal to CA large loading condition. In this case, the damage caused by σ_L is 0, while the damage caused by σ_H is 1, and then D_{nl} is equal to 0. In other words, there is no interaction effect between the high and low amplitude loads, which is consistent with the fatigue performance of DTS under CA load.

According to the Eq. 3, the values of D_{nl} in different cycle ratio conditions can be calculated, as shown in Table 6. In each cycle ratio, the numbers of low amplitude load cycles and high amplitude load cycles are the mean values of valid experimental data. From Table 6, it can be seen that when the cycle ratios are 1:1 and 2:1, D_{nl} are very small with the values of 0.057 and 0.047, respectively, which indicates that the fatigue damage of the low and high amplitude loads is linear in these two cycle ratio conditions. When the cycle ratios are 3:1 and 4:1, the values of D_{nl} are 0.241 and 0.303, which indicates that the loading interaction effect is harmful to the fatigue life of the material and can't be ignored. Furthermore, it can be seen that the value of D_{nl} is much greater than the fatigue damage caused by the low amplitude load in these two cycle ratio conditions. When the cycle ratios are 4.5:1 and 5:1, the values of D_{nl} are -0.011 and -0.120, which indicates that the loading interaction has a beneficial effect on the fatigue life of the material. This characteristic of D_{nl}, which changes with the cycle ratio increasing, can give a reasonable explanation to the phenomenon that both the cycle numbers of low and high amplitude loads increase with the cycle ratio increasing after n_{L}/n_H is greater than 4.

In order to analyze the reason for the value of D_{nl} variation with the cyclic ratio increasing, one kind of microscopic analysis methods, the X-ray Diffraction (XRD) analysis was adopted to observe the microstructural evolution at the crack initiation area in different cycle ratio conditions [34]. Fig. 12 shows the XRD patterns of the crack initiation area in different cycle ratio conditions. The XRD patterns of each working condition are very almost coincident, so one of the samples in each working condition was selected for comparison. It can be seen that the diffraction peak of the body-centered cubic (110) crystal plane of Q345B high strength steel is the most obvious. In order to investigate microstructure evolution in different cycle ratio conditions, Rachinger method was carried out to subtract the backgrounds and separate the $K_{\alpha 2}$ from XRD patterns. Fig. 13 shows the normalized $K_{\alpha 1}$ components of (110) crystal plane of crack initiation area in different cycle ratio conditions. Because of different surface conditions of fatigue specimens with different cycle ratios, the backgrounds of diffraction profile shown in Fig. 12 are different. As a result, it can be seen that there is a fluctuation of the height of FWHM (the full width at half maximum). The fluctuation of the height of FWHM is a common phenomenon in XRD tests and this phenomenon does not affect the analysis of material microstructure such as grain size and work hardening state or work softening state. In the XRD analysis, the value of FWHM of the characteristic peak is a very important

physical parameter to evaluate the material grain size at the microcrack tip region. The FWHM of (110) crystal plane increases firstly and then decreases with increasing the cycle ratio from 1:1 to 5:1. Specifically, the mean values of FWHM of (110) crystal plane under different cycle ratio are 0.33,0.39, 0.53, 0.65, 0.47 and 0.43, respectively, when the cycle ratios are 1:1, 2:1, 3:1, 4:1, 4.5:1 and 5:1.

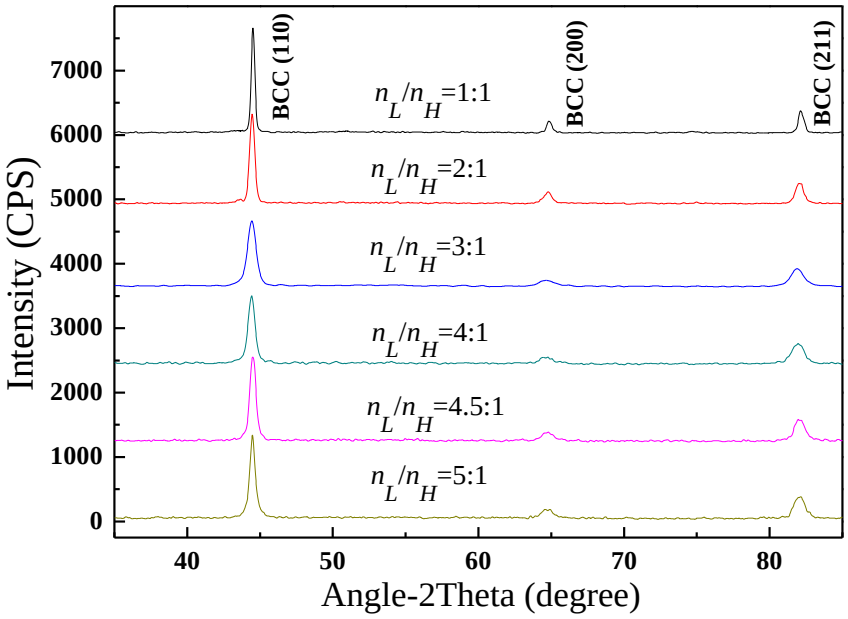

Fig. 12. The XRD pattern of the crack initiation area under different cycle ratio

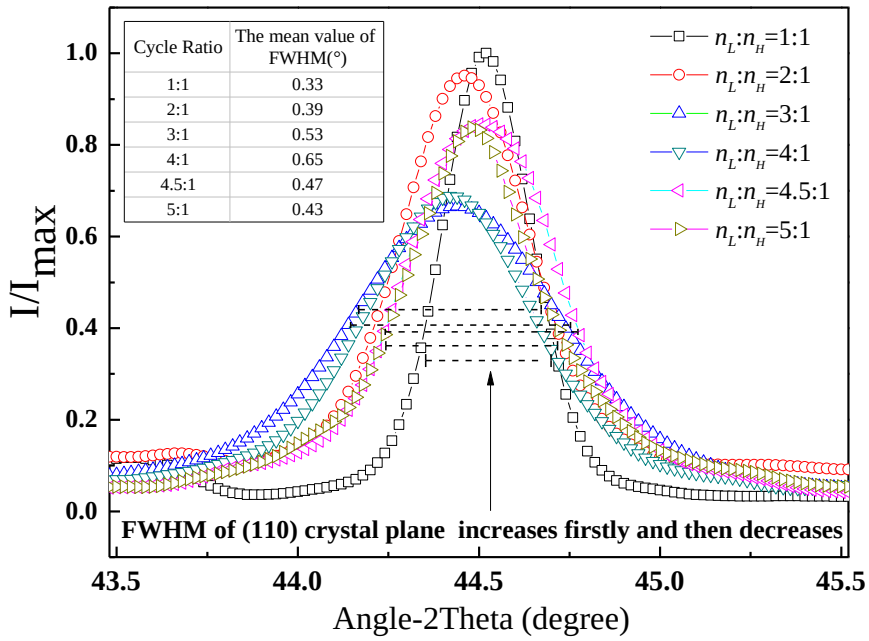

Fig. 13. The normalized $K_{\alpha 1}$ components of (110) crystal plane of crack initiation area under different cycle ratio

It is well known that the value of FWHM represents the amount of dislocation density in material. The larger the FWHM is, the greater the dislocation density inside the material is. Work-hardening state of material represents the dislocation density increases in the material, which make the characteristic peaks broaden in the XRD pattern. In the crack initiation area, the microcrack tip propagates continuously during cyclic loading. When the cycle ratio is less than 4, the work-

hardening phenomenon appears at the crack tip because of repeated low amplitude loading on this small area. According to the Baily-Hirsch equation [35, 36], the yield strength of materials can be calculated based on the dislocation density as follows:

$$\sigma_Y = \sigma_0 + \beta\mu b{\rho_D}^{1/2} \tag{4}$$

where σ_Y is the yield strength of work-hardening-state metal, σ_0 is the yield strength of the annealed metal, β is a constant, μ is the shear modulus of metal, b is the Burgers vector of dislocations, and ρ_D is the dislocation density. From Baily-Hirsch equation, it can be seen that the yield strength of materials is directly proportional to the square root of dislocation density. Work-hardening state of the microcrack tip leads to material strength and hardness increasing but ductility decreasing at this area, which leads to the rate of microcrack propagation increasing. Therefore, the value of D_{nl}, which represents fatigue damage due to the interaction effect between the high and low amplitude loads during fatigue tests, increases with the rate of microcrack propagation increasing.

With the cycle ratio increasing greater than 4, dislocations with opposite signs annihilate each other at microcrack tip area, where the high dislocation density has already existed because of work-hardening. The dislocations annihilation phenomenon leads to the dislocation density decreasing at the microcrack tip. This fact is confirmed by the characteristic peaks in XRD pattern becoming sharper again. The decrement of dislocation density represents the work-softening phenomenon appearing at the microcrack tip. The work-softening phenomenon leads to the material strength and hardness decreasing but ductility increasing at the microcrack tip, which leads to the rate of microcrack propagation decreasing. The value of D_{nl} decreases with the rate of microcrack propagation decreasing. When the cycle ratios are 4.5:1 and 5:1, the value of D_{nl} is negative, which indicates that it is beneficial to material fatigue property if increasing the cycle number of low amplitude load. The better fatigue property is mainly due to the work-softening state appearing at the microcrack tip in the crack initiation area when the cycle ratio is relatively larger, which leads to the rate of microcrack propagation decreasing drastically.

5. Conclusion

In order to investigate the fatigue damage evolution of the structural components of the RSGS under repeating two-step VA loading condition, and to estimate the influence of the damage of low amplitude load below the fatigue limit and the interaction effect between the high and low amplitude loads on the fatigue life of the structure, a series of fatigue experiments of the Q345 steel DTS were carried out in this work**.** The interaction damage value (D_{nl}), which reflected the interaction effect between two-step VA load on fatigue property, was proposed firstly based on the Palmgren-Miner linear damage rule. The following conclusions have been reached:

1. The Palmgren-Miner linear damage rule can't accurately evaluate the cumulative damage of the DTS under repeating two-step VA load, and the effect of loading interaction can't be ignored when the cycle ratio (n_L/n_H) is larger than 3. When the loading cycle ratio is less than 4, the interaction damage value (D_{nl}) caused by loading interaction is positive, which indicates that the loading interaction effect is harmful to the fatigue life of the DTS. On the contrary, the value of D_{nl} is negative when the cycle ratio is larger than 4.5, which indicates that the loading interaction has a gain effect on the fatigue life.

2. According to the XRD analysis of the fracture in the crack initiation area, the material at the microcrack tip changes from the work-hardening state to the work-softening state with increasing the cycle ratio. The work-hardening state at the microcrack tip can increase the rate of microcrack propagation while the work-softening state can decrease the rate of microcrack propagation. The value of D_{nl} is closely related to the work-hardening and work-softening states of the material at the microcrack tip caused by low amplitude load below the fatigue limit under the two-step VA repeating loading condition.

Acknowledgements

This research was funded by the National Natural Science Foundation of China (No. 51879208) and the National Scientific Research Project of the High-tech Ship of China (No.2014【493】). The authors are grateful to all the staff of Hubei Province Engineering Research Center on Green & Smart River-sea-going Ship for fatigue test and Dr. Chunhua Shen from the Center for Materials Research and Analysis, Wuhan University of Technology for XRD analysis.

Reference

[1] Cui WZ, Cai XG, Leng JX. A State of the Art Review for the Fatigue Strength Assessment of Ship Structures. Journal of Ship Mechanics. 19984): 63-81.

[2] Sun D, Gan J, Wang Z, et al. Experimental and analytical investigation of fatigue crack propagation of T-welded joints considering the effect of boundary condition. Fatigue & Fracture of Engineering Materials & Structures. 2017, 40(6): 894-908.

[3] He L, Akebono H, Kato M, et al. Fatigue life prediction method for AISI 316 stainless steel under variable-amplitude loading considering low-amplitude loading below the endurance limit in the ultrahigh cycle regime. International Journal of Fatigue. 2017, 101: 18-26.

[4] Gates N R, Fatemi A. Fatigue Life of 2024-T3 Aluminum under Variable Amplitude Multiaxial Loadings: Experimental Results and Predictions. Procedia Engineering. 2015, 101: 159-168.

[5] Sakai T, Nakagawa A, Oguma N, et al. A review on fatigue fracture modes of structural metallic materials in very high cycle regime. International Journal of Fatigue. 2016, 93: 339-351.

[6] Zhang M, Wang W, Wang P, et al. Fatigue behavior and mechanism of FV520B-I welding seams in a very high cycle regime. International Journal of Fatigue. 2016, 87: 22-37.

[7] Yang F, Yin SM, Li SX, et al. Crack initiation mechanism of extruded AZ31 magnesium alloy in the very high cycle fatigue regime. Materials Science and Engineering: A. 2008, 491(1-2): 131-136.

[8] Grad P, Reuscher B, Brodyanski A, et al. Mechanism of fatigue crack initiation and propagation in the very high cycle fatigue regime of high-strength steels. Scripta Materialia. 2012, 67(10): 838-841.

[9] Gan J, Sun D, Wang Z, et al. The effect of shot peening on fatigue life of Q345D T-welded joint. Journal of Constructional Steel Research. 2016, 126: 74-82.

[10] Radmilović Z, Zobenica R, Maraš V. River-sea shipping competitiveness of various transport technologies. Journal of Transport Geography. 2011, 19(6): 1509-1516.

[11] Charles L. Sea–river shipping competitiveness and its geographical market area for the Rhône−Saône corridor. Journal of Transport Geography. 2008, 16(2): 45-116.

[12] Xu F. Study on fatigue performance of river-sea container ship. Jiangsu University of Science and Technology, 2016.

[13] Gao XY, Sun D. Experimental Study on Fatigue Characteristics of Typical Welded Joints of River-Sea-Going

Ship. 2017.
[14] Miner M. Cumulative damage in fatigue. Trans ASME. 1945(67): A159-A164.
[15] Palmgren A. Endurance of ball bearings. Z Ver Deutsch Ing. 1924(68): 339-341.
[16] Yao WX. Fatigue life prediction of structures. Beijing: National Defence Industry Press, 2002: 35-36.
[17] Mayer H. Fatigue damage of low amplitude cycles in low carbon steel. Journal of Materials Science. 2009(No.18): 4919-4929.
[18] Mayer H, Ede C, Allison J E. Influence of cyclic loads below endurance limit or threshold stress intensity on fatigue damage in cast aluminium alloy 319-T7. International Journal of Fatigue. 2005, 27(2): 129-141.
[19] Jono M, Hanai M, Kikukawa M. Effect of frequency ratio of overstress to understress on cumulative damage below fatigue limit. Educational Measurement Issues & Practice. 2010, 29(1): 25-37.
[20] Lu X, Zheng SL. Strengthening of transmission gear under low-amplitude loads. Materials Science & Engineering A. 2008, 488(1): 55-63.
[21] Lu X, Zheng SL. Changes in mechanical properties of vehicle components after strengthening under low-amplitude loads below the fatigue limit. Fatigue & Fracture of Engineering Materials & Structures. 2009, 32(10): 847-855.
[22] Nakajima M, Jung J W, Uematsu Y, et al. Coaxing Effect in Stainless Steels and High-Strength Steels. Key Engineering Materials. 2007, 345: 235-238.
[23] Pereira HFSG, Jesus AMPD, Ribeiro AS. Cyclic and fatigue behavior of the P355NL1 steel under block loading. Journal of Pressure Vessel Technology. 2009, 131: 021210-021218.
[24] Rege K, Pavlou D G. A one-parameter nonlinear fatigue damage accumulation model. International Journal of Fatigue. 2017, 98: 234-246.
[25] Ciavarella M, D'Antuono P, Demelio G P. A simple finding on variable amplitude (Gassner) fatigue SN curves obtained using Miner's rule for unnotched or notched specimen. Engineering Fracture Mechanics. 2017, 176: 178-185.
[26] Lv ZQ, Huang HZ, Zhu SP, et al. A modified nonlinear fatigue damage accumulation model. International Journal of Damage Mechanics. 2015, 24(2): 168-181.
[27] Ye DY, Wang ZL. A new approach to low-cycle fatigue damage based on exhaustion of static toughness and dissipation of cyclic plastic strain energy during fatigue. International Journal of Fatigue. 2001, 23: 679–687.
[28] Correia JAFDO, Jesus A, Blason S, et al. Probabilistic Non-Linear Cumulative Fatigue Damage of The P355NL1 Pressure Vessel Steel. Proceedings of the ASME Pressure Vessels and Piping Conference. 2016, 6A: 1-9.
[29] Zhu SP, Hao YZ, Correia JAFDO, et al. Nonlinear fatigue damage accumulation and life prediction of metals: A comparative study. Fatigue & Fracture of Engineering Materials & Structures. 2019, 42(6): 1271-1282.
[30] Tang ZT. General Methods for Outlier Detection in Metal Fatigue Tests. Civil Aircraft Design & Research. 2017(1):77-82.
[31] Lu X, Zheng SL. Strengthening and damaging under low-amplitude loads below the fatigue limit. International Journal of Fatigue. 2009(2): 341-345.
[32] Ngiau C, Kujawski D. Sequence effects of small amplitude cycles on fatigue crack initiation and propagation in 2024-T351 aluminum. International Journal of Fatigue. 2001, 23(9): 807-815.
[33] Gao HY, Huang HZ, Zhu SP, et al. A Modified Nonlinear Damage Accumulation Model for Fatigue Life Prediction Considering Load Interaction Effects. The Scientific World Journal. 2014, 2014: 1-7.
[34] B.E.Warren. X-Ray Diffraction．NEW YORK：DOVER PUBLICATIONS, INC. 1990：251-254.
[35] Feng D. Metallic Physics: Metal Mechanical Property. Beijing: Science Press, 1999.
[36] Lai ZH. Crystal Defect and Mechanical Properties of Metals. Beijing: Metallurgical Industry Press, 1998.